JOURNAL OF
REINFORCED
PLASTICS &
COMPOSITES

Original article

Journal of Reinforced Plastics and Composites
0(0) 1–15

DOI: 10.1177/0731684418770528
journals.sagepub.com/home/jrp
SAGE

Development of the layered structure in a double-gated glass fiber-reinforced polypropylene injection molding: Experimental and simulated results

MC Quintana and MP Frontini

Abstract

The present study aims to experimentally validate numerical simulation of fiber orientation distribution performed by molding simulation software Moldex3D in a double-gated injection-molded glass fiber-filled (40 wt%) polypropylene box, by making a detailed comparison of predicted and experimentally measured fiber orientation distribution data. The modeling approach evaluated in this work consists in the implementation of the Folgar–Tucker rotary diffusion model with the invariant-based optimal fitting closure approximation for the fourth-order orientation tensor. The specimen used has a weld line in the center and sharp corners. This investigation characterizes in detail the development of the through-thickness layered structure at distinctive locations of the specimen. The sensitivity of fiber orientation distribution and the layered structure to changes upon injection time and melt temperature is also evaluated. The boxes display the typical layered laminate structure, with fibers aligned in the main flow direction near the walls (shell layer) and less oriented in the middle plane (core layer). The boxes injected at the lowest melt temperature display an additional skin layer. Unfortunately, simulation fails in predicting the five layers structure developed under these latter conditions. The grade of fiber orientation is deemed to be independent of process parameters but not the layered structure.

Keywords

Polymer–matrix composites, injection molding, microstructure analysis, process simulation

Introduction

Injection-molded discontinuous fiber-reinforced thermoplastics (FRTs) are widely considered by many industrial areas because of their specific mechanical properties, i.e. a high strength-to-weight ratio, especially by the automotive industry to the reduction of fuel consumption. However, the actual improvement with respect to the use of a neat polymer in the performance of an injection component will depend upon the flow-induced fiber orientation. When the flow develops with high shear stresses the fibers tend to align in the flow direction, whereas a predominantly extensional flow tends to align the fibers in the principal extension direction. In consequence, injection-molded FRT components exhibit a distinct laminate structure of fiber orientations across their thickness.[1–11]

The variations of part properties associated to the inherent anisotropy produced by the fibers are much more pronounced in those parts having local disruptions of the global filling pattern, such as weld lines (WLs) and sharp corners.[10,12–17] This is due to the fact that the fiber orientation at these geometrical singularities is fundamentally different from the orientation in the rest of the part.

Therefore, in order to optimize and control the technology of injection molding of FRT, it is crucial to understand and to be able to predict the dynamics of flow and fiber orientation not only as a function of material parameters and process conditions, but also as

Instituto de Investigaciones en Ciencia y Tecnología de Materiales (INTEMA)—Universidad Nacional de Mar del Plata, Mar del Plata, Buenos Aires, Argentina

Corresponding author:
MC Quintana, Universidad Nacional de Mar del Plata, B7608FDQ, Av. Juan B. Justo 4302, Mar del Plata 7600, Buenos Aires, Argentina.
Email: cquintana@fi.mdp.edu.ar

a function of the mold geometry and geometrical flow pattern.

To verify the trustworthy of predictive models implemented in computational codes, it is necessary to perform laborious experimental determinations or measurements.[18,19] There are many sound works in the specific literature which attempted to establish the correlation between material, processing parameters, mold geometry, and the resulting fiber orientation in injected parts. An excellent review on the subject of the computational studies on fiber orientation in injection molding of fiber-reinforced composites has been made by Papthanasiou.[10] Despite the great contribution already made by previous works regarding the comprehension of the phenomena, due to the inherent complexity of this relationship, most of the investigations are still limited to the analysis of rather simple analytical or standard geometries like the end-gated rectangular plate or the center-gated disk.[20–23]

Taking into account the above statement, the main objective of this work is to study the fiber orientation distribution (FOD) characteristics in a geometry which displays a WL in the center and has sharp corners that may constitute a potential lateral boundary effect for fiber orientation. We have sought to establish through a detailed experimental study the state of orientation within these geometric discontinuities and the precision of the commonly used orientation model (Folgar–Tucker (FT)) to describe such orientation characteristics. According to traditional usage a default value for the interaction coefficient (Ci = 0.001) has been selected. We also attempt to clearly establish the advantages and limitations of the prediction approach—FT rotary diffusion model with modified invariant-based optimal fitting (IBOF) closure approximation for the fourth-order orientation tensor—to provide valuable and novel information that could be used in the analysis of the orientation state of even more complex pieces. The fiber orientation pattern along the flow, cross flow, and through-thickness directions is deeply studied to denote distinctive fiber orientation zones in the geometry. Besides, the through-thickness layered structure developed in the box as a function of the location is particularly analyzed in detail.

On the other hand, since it is widely established that injection parameters exert a profound influence on the morphology of the polypropylene composites,[24–26] an additional objective of the present paper was to evaluate the parametric sensitivity of FOD to changes in process conditions. Particularly, this study is concerned about analyzing the effect of injection time and melt temperature on the final state of fiber orientation, both in the degree of orientation and in the layered nature of fiber orientation across the box thickness. We face the problem by studying the combined influence of the processing variables, and not their individual contribution, given that the effects of each parameter in a thermomechanical process of this complexity are not easy to be isolated.

Background

Governing equations and fiber orientation description

The orientation of a single fiber is described by a unit vector along its axis direction, named p. The orientation state of a group of fibers is given by a second-order orientation tensor, A_{ij}, equation (1)

$$A_{ij} = \int \left(p_i p_j\right)\psi(\mathrm{p})\mathrm{dp} \tag{1}$$

where ψ is the probability density distribution function over the orientation space, defined so that the probability of a fiber being oriented within an angular range d$\mathbf{p}$ of the direction $\mathbf{p}$ is equal to $\psi(\mathbf{p})$d$\mathbf{p}$.

The elements of the second-order tensor have a physical meaning. The value of each of the diagonal elements of the tensor stands for the relative orientation in one of the coordinate axes. The sum of the diagonal terms of the tensor is the unit, and each of the diagonal values is allowed to vary between 0 and 1.

The evolution equation of the second-order orientation tensor, proposed by Advani and Tucker,[4] is given in equation (2)

$$\begin{aligned}\frac{\partial A_{ij}}{\partial t} + u_k \frac{\partial A_{ij}}{\partial x_k} &= A_{ij}\Omega_{kj} - \Omega_{ik}A_{kj} \\ &+ \lambda(A_{ik}E_{kj} + E_{ik}A_{kj} - 2A_{ijkl}E_{kl}) \\ &+ 2C_I\dot{\gamma}(\delta_{ij} - 3A_{ij})\end{aligned} \tag{2}$$

where E and Ω are the strain rate and vorticity tensors, respectively; u_k is the velocity component; λ is a constant that depends on the geometry of the part in this work $\lambda = 1$, that is the value corresponding to slender particles; δ_{ij} is the unit tensor; γ is the scalar magnitude of E; and C_I is the interaction coefficient whose value ranges from 10^{-2} to 10^{-3}.

Equation (2) includes the theoretical models of Jeffery's hydrodynamic (HD),[1] for dilute suspensions, and the Folgar and Tucker's isotropic rotary diffusion (IRD),[2] that add a rotary diffusivity term ($D_r = C_I\dot{\gamma}$) to model the randomizing effect of fiber–fiber interactions. In general, the combination of the HD model with the IRD model is called the standard FT orientation equation, which is expressed in the second-order orientation tensor A_{ij}.

Table 1. Material properties.

Modulus E1 (fiber direction) (GPa)	7
Modulus E2 (transverse direction) (GPa)	4
Shear modulus G (GPa)	1.45
Poisson's ratio	0.38
Fiber length/diameter (L/D)	30
Fiber weight percentage (%)	40

For the fourth-order tensor A_{ijkl}, a closure approximation, which allows to expressing A_{jkl} in terms of the components of the second-order tensor A_{ij}, is needed in order to obtain a closed set of equation.

Experimental

Material

The material of this study is a 40 wt% glass fiber-filled polypropylene, grade name Hostacom G4 R01 produced by Lyondell Basell. Material properties are given in Table 1. These properties are extracted from Moldex3D material database and are provided by the manufacturer.

Injection molding: Cavity geometry and processing conditions

Injection-molded box geometry and its dimensions are shown in Figure 1. The base of the box (bottom plane) is 70 mm by 130 mm, the height of the wall is 15 mm, and the part thickness is 1.4 mm.

The boxes were injected in a hot runner injection machine *Klockner-Ferromatik Desma FM20* of clamping force 200 kN. For further technical details on the injection of these specimens—which was done in a previous work—the reader is referred to Gamba et al.[16] The values of the injection molding parameters are listed in Table 2.

Four different processing conditions arise of the combination of the melt temperatures (Tm) 250 and 280°C and the injection times (ti) 0.5 and 1.5 s (see Table 3).

Samples location and preparation

Figure 2 shows the location of the samples taken from the boxes for examination of fiber orientation. One box per processing condition was randomly selected and its bottom plane was transversely divided into three regions of interest, namely: region 1—the entrance region, at the injection point (IP) zone; region 2—the lubrication region, located between IP zone and WL zone; and region 3—the WL zone. In order to determine if fiber orientation is affected by the presence of the box walls, the above referred regions (regions 1–3) were further subdivided longitudinally into two zones, namely center and border zones. As a result of the divisions, a total of six samples were obtained for each processing condition.

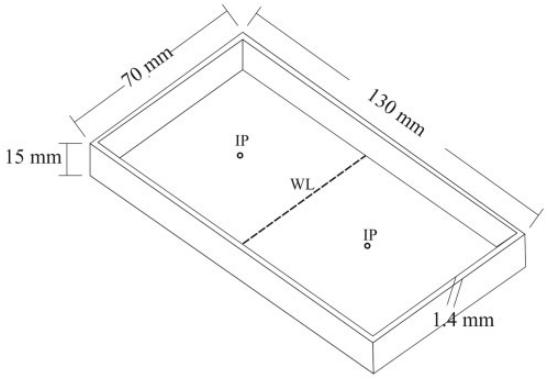

Figure 1. Injection molding box geometry and dimensions. IPs and WL.

Table 2. Injection molding parameters.

Melt temperature (Tm, °C)	250 and 280
Injection time (ti, s)	0.5 and 1.5
Injection pressure (Pi, MPa)	3
Holding pressure (Ph, MPa)	1.8
Mold temperature (Tmold, °C)	50

Table 3. Processing conditions.

Condition	Tm (°C)	ti (s)
(i)	250	0.5
(ii)	250	1.5
(iii)	280	0.5
(iv)	280	1.5

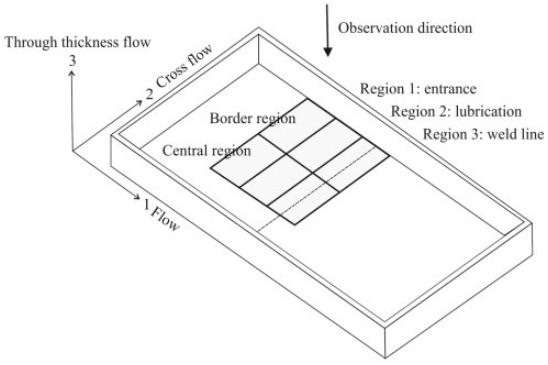

Figure 2. Samples location and observation direction.

The samples were cut using a handsaw and mounted (glued) on individual supports, identifying its position relative to the directions 1 and 2, as indicated. Then they were subjected to successive stages of metallurgical polishing (sandpaper of progressively smaller roughness) to achieve a microscopically smooth surface. Each sample was subjected to four stages of polishing—approximately until its midplane—giving as a result four cross sections per sample to be microscopically analyzed.

The relative through-thickness position of the analyzed polished cross sections, i.e. in direction 3, is denoted as "z/H," being "z" the position of the 1–2 plane in direction 3 and "H" the thickness of the samples. In the successive figures, location of the layers is also denoted with the letter "L" followed by the number of the layer analyzed.

Measurement of fiber orientation: Method of ellipses

The remaining surface of each stage of polishing was examined and photographed using a reflective light optical microscope Olympus BH2. The enlargement of micrographs was 1:50. The sections of the fibers appear in the images as circles if the fibers are aligned in a direction perpendicular to the polishing plane, rectangles if the fibers are parallel to the polishing plane, or as ellipses otherwise.[18,19,27] The out-of-plane orientation angle θ is derived from the major M and minor m axes of the ellipse as shown in equation (3)

$$\theta = arcos\left(\frac{m}{M}\right) \tag{3}$$

The in-plane orientation angle ϕ is defined by the major axis of the ellipse and the selected reference axes, direction 1 in our case (see Figures 2 and 3).

Angles θ and ϕ were determined by digitizing the coordinates of the end points of the major and minor axes of the ellipses using an image analysis tool (Image J).

The Cartesian components of the vector p as a function of θ and ϕ are given in equations (4) to (6)

$$p_1 = \sin\theta \cdot \cos\phi \tag{4}$$

$$p_3 = \sin\theta \cdot \sin\phi \tag{5}$$

$$p_3 = \cos\theta \tag{6}$$

The components of the second-order tensor for a group of n fibers are calculated as a function of p as shown in equation (7)

$$a_{ij} = \sum_n (p_i)_n (p_j)_n \tag{7}$$

After image processing and calculation, the average orientation tensors layer by layer in direction 3 were obtained. The results are displayed in this work in line plots of the principal components of the orientation tensor as a function of the through-thickness position, in order to be compared with the predicted values.

Numerical simulation

Implementation details

Moldex3D CFD software was used to perform the three-dimensional fiber orientation simulation concurrent with the mold filling analysis on the same finite element mesh. For filling simulation, material properties were obtained from Moldex3D materials database (see Table 1), and the process setting was made accordingly to the real process parameters (see Table 2).

FT model has been implemented for the prediction of the fiber orientation state and the computation of the components of the second-order orientation tensor. This model gives acceptable accuracy for the prediction of fiber orientation in concentrated (semidiluted)

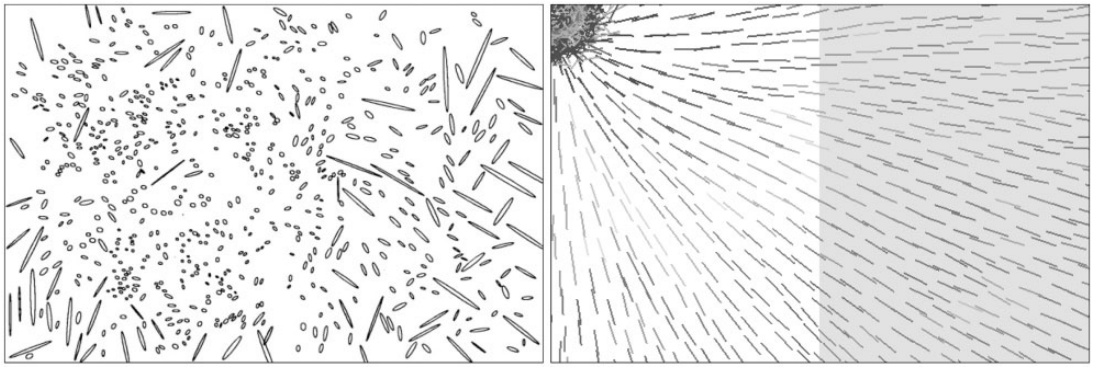

Figure 3. Fiber orientation at the entrance region (center region 1). Left: experimental results. Right: simulation results.

suspensions.[2] As explained in the "Background" section, the FT model takes account of fiber–fiber interaction by means of an IRD term ($D_r = C_I\gamma$). Regarding the interaction coefficient C_I, there have been several attempts to establish an empirical model for its value, but still there is not an accepted method to find this parameter.[19] There is not yet a detailed model that describes the transient interactions between fibers.[28] However, through the experimental evaluation of the interaction coefficient by fitting the predictions to fiber orientation data from injection molding, has been stated that the range of values for C_I is from 10^{-2} to 10^{-3}.[29] Since experimental orientation showed up to be highly oriented and taking i to account that low values of interaction coefficient represents highly aligned states, CI was taken as 0.001.

For the fourth-order orientation tensor closure, Moldex3D includes three methods: Hybrid (Original Moldex3D fiber orientation calculation solver model), orthotropic fitted closure approximation (ORE), and IBOF closure approximation. The IBOF model is implemented in this work since it has been demonstrated that it is able to improve the problem of fiber orientation tensor overestimation that occurs when using the hybrid model and it requires a shorter computation time than ORE model.[30,31]

Results and discussion

Qualitative description of fiber orientation along main and cross flow directions

Figures 3 to 5 present the qualitative comparison of predicted and experimental FOD along the main flow direction for regions 1–3. The analysis is done for the 1–2 plane located at z/H = 0, i.e. at the bottom plane of the boxes and is focused on its central zone. The results are shown only for one condition Tm = 280°C and ti = 0.5 s, since the results obtained for the other conditions are analogous. The images on the left are the processed images—by means of the image analysis software—of the micrographs taken at the analyzed plane, while the right images correspond to the simulated results, in which the orientation of the short lines indicates the most favorable orientation direction and the displayed gray value represents the degree of orientation in that direction (a darker gray value means more oriented). The border zone is displayed shaded

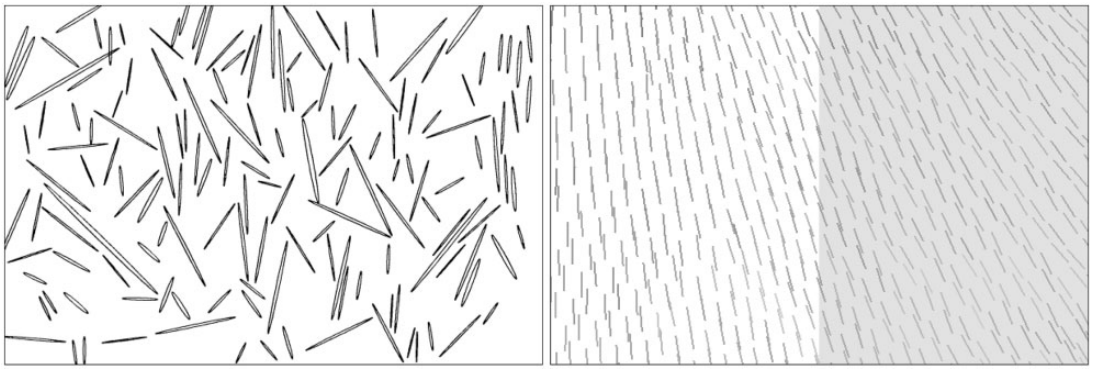

Figure 4. Fiber orientation at the lubrication region (center region 2). Left: experimental results. Right: simulation results.

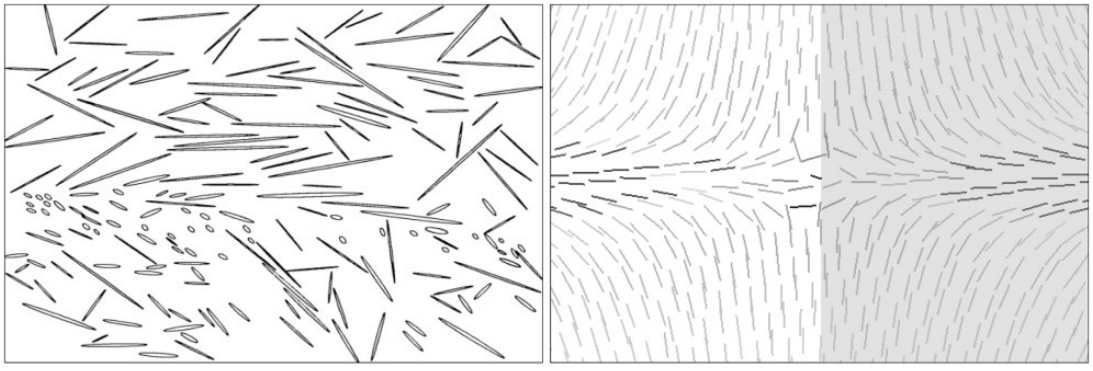

Figure 5. Fiber orientation at the WL region (center region 3). Left: experimental results. Right: simulation results.

in simulated images because it is not taken into account in this part of the study.

From the observation of the experimental and the simulated fiber orientation patterns, it can be seen that fibers follow a radial divergent flow path (as in a center-gated disk) that starts at each IP and ends with the contact of the flow fronts at the WL zone. As it is explained in the specific literature,[10] the orientation pattern is the result of the combination of shearing flow that tends to align fibers in the direction of flow and in-plane stretching flow that tends to align fibers in the stretching direction. In our case, the stretching axis is perpendicular to the radial flow direction. Accordingly, along the flow direction, three regions where fibers follow a preferential direction can be distinguished: The entrance region, where fibers align evenly in the main and cross flow directions—this corresponds to the radial alignment in a polar coordinate system; the lubrication region, where fibers orient parallel to the main flow direction; and the WL region, where fibers are aligned in the cross flow direction. As it can be appreciated, each of this distinctive alignment zones corresponds to regions 1–3 in which boxes were divided to do the experimental measures.

Regarding to the cross flow direction, two analyses are carried out: the change of the fiber orientation with respect to the distance to the longitudinal center of the boxes and the fiber orientation at the WL.

Figures 6 to 8 show the comparison of predicted and experimental FOD along the cross flow direction for regions 1–3. The analysis is also done for the 1–2 plane located at $z/H = 0$, but it is focused on the border zone of the boxes. The results shown correspond to the same condition chosen in the flow direction analysis in order to be compared. Here, the images on the left are the simulated results—the central zone is shaded in this case—and ones to the right are the experimental results.

The images show that as the distance to the center zone increases, the fibers change gradually their orientation from being aligned along the flow direction to being aligned along the cross flow direction following the radial divergent flow path (see Figures 6 to 8 with respect to Figures 3 to 5 for comparison). This is due to the fact that the elongational stresses become predominant over the shear stresses toward the edge. In addition, the through-thickness layered nature of the fiber orientation also changes with the radial

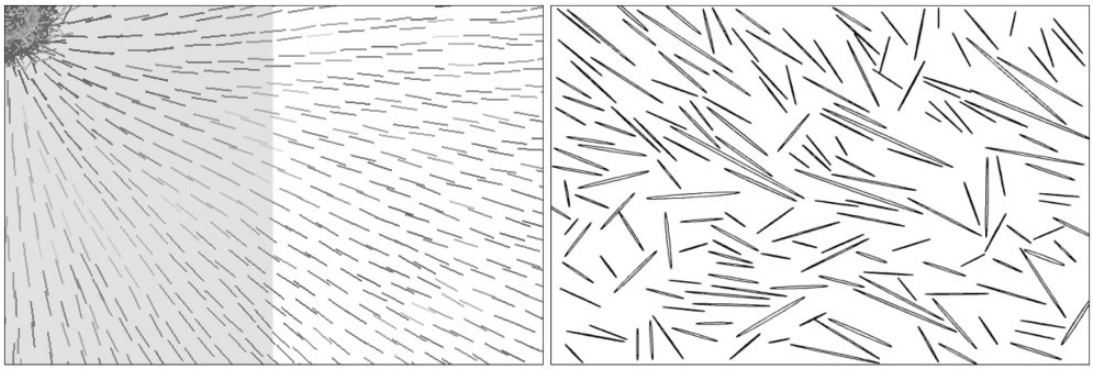

Figure 6. Fiber orientation at the entrance region (border region 1). Left: simulation results. Right: experimental results.

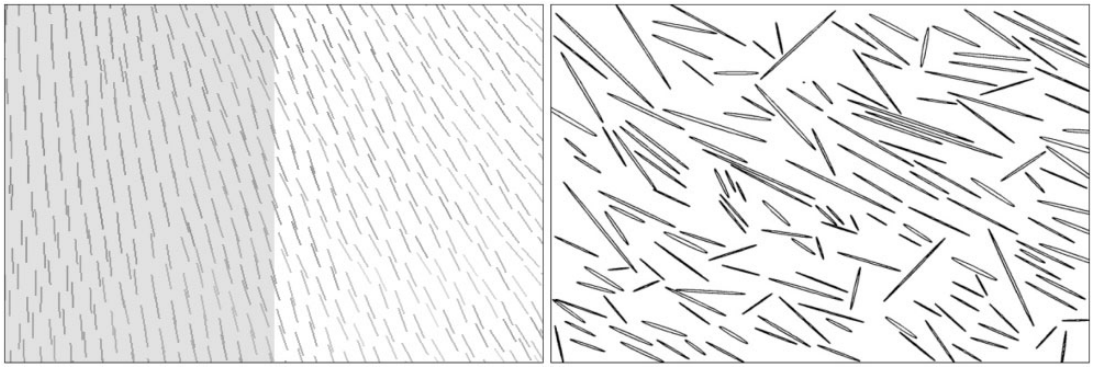

Figure 7. Fiber orientation at the lubrication region (border region 2). Left: simulation results. Right: experimental results.

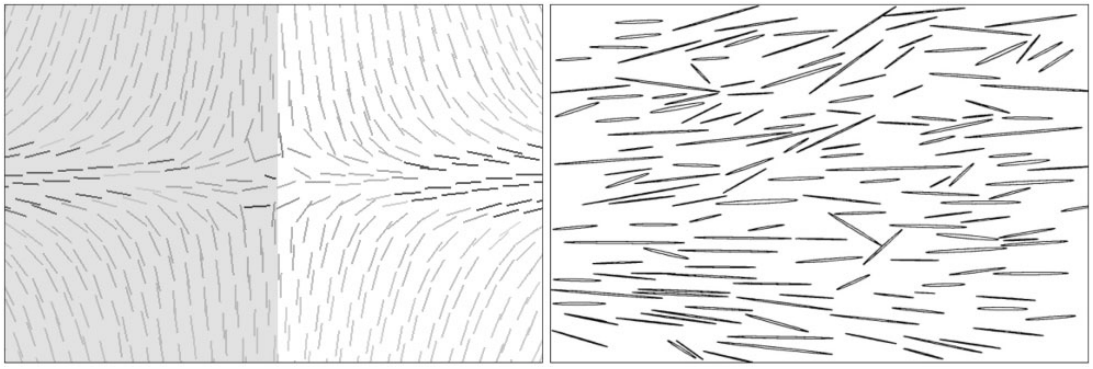

Figure 8. Fiber orientation at the WL region (border region 3). Left: simulation results. Right: experimental results.

distance to the IP: the proportion of fibers oriented in the main flow direction decreases until most of the fibers align in the cross flow direction upon reaching the edge of the box. The variation in the through-thickness orientation along the cross flow direction can be seen in Figure 9, which corresponds to the simulated fiber orientation for a 2–3 plane located at an arbitrary position at the lubrication region. In the figure, it can be seen the transition between fibers oriented along flow direction (dots), fibers less oriented along flow direction (short lines), and fibers completely oriented along the cross flow direction (longer lines).

Figure 10 shows another result that arises from the experimental and simulated results observation concerning the border region. This is that the fibers do not align with the joint between the base and the wall of the box, i.e. in direction 1, when it reaches this edge, but its orientation continues to be along the cross flow direction. Note that this is different from what it was observed by Papthanasiou[10] for the center-gated disk—that also has a radial divergent flow pattern as mentioned earlier—who described that fibers align in the border direction.

Figures 5 and 8 show the fiber orientation at the WL region—accordingly to the observation direction indicated in Figure 2—for the center and border regions, respectively. It can be seen that the fibers align predominantly in the cross flow direction from the center to the border regions, as a consequence of the volcano-like mechanism which creates orientation at 90° angle to main polymer flow direction. The experimental image in Figure 5—that to the left—displays some fibers oriented out of plane—that appears as dots—at the precise region where the two flow fronts impinge head-on. The orientation of the fibers has been found to be transversal to the main flow direction not only across the entire width of the WL but also through its thickness, meaning that the gap-wise structure of different fiber alignments is not distinguishable here. This can be seen clearly in Figure 11 that shows the simulated fiber orientation for a 2–3 plane located at the center of the WL region.

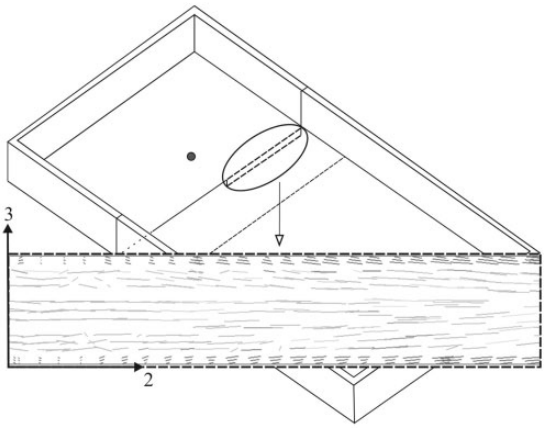

Figure 9. Predicted through-thickness fiber orientation along the cross flow direction at the lubrication region.

Experimental through-thickness FOD

Due to the shearing/stretching nature of radial flow, extensively explained in literature,[3,5–10] the fibers tend to align following the cross flow direction near the mid-plane of the injected part—i.e. transversally—forming the core region, but aligned with the main flow direction near the surface of the part—i.e. radially—forming the shell region. Besides the shell–core–shell structure, a thin layer of in-plane randomly oriented fibers is sometimes found at the surface of molded parts, immediately adjacent to the mold surface. This lower oriented region, named skin layer, is caused by fountain flow near the melt font which moves material (including fibers) from the core to the cavity walls where it freezes before gap-wise shearing is able to align the fibers in the flow direction.[6,10] Given the through-thickness distribution of fiber orientations, the short fiber-reinforced box studied has a gap-wise layered nature.

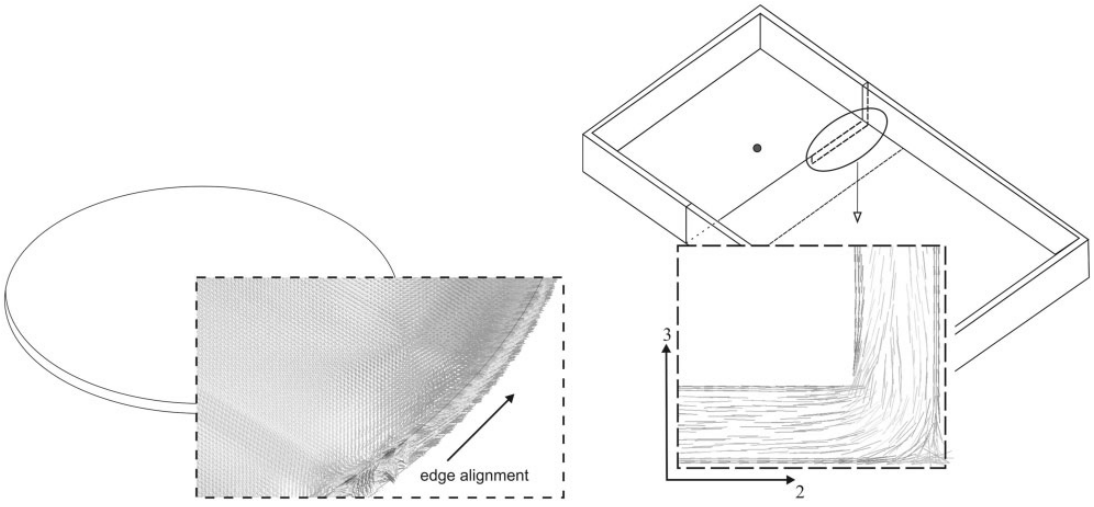

Figure 10. Comparison of fiber orientation at the edge of the specimen in radial divergent flow geometries. Left: disc displaying edge alignment. Right: joint between box's base and wall without edge alignment.

Figures 12 to 14 display typical features of the experimental measured through-thickness fiber orientation for the three regions of interest. The important orientation descriptors are the orientation tensor components: a_{11}, a_{22}, and a_{33} corresponding to the flow, the cross flow, and the thickness directions, respectively. In general, a high value of a_{11} indicates a large fraction of fibers oriented in the flow direction, a high value of a_{22} indicates a large fraction of fibers oriented in the cross flow direction, whereas a near-zero value of a_{33} would indicate little or no orientation in the thickness direction. In these figures, the vertical lines at the beginning and at the end of the through-thickness profiles of the principal components of the orientation tensor were drawn so that it would be possible to better understand the proportionality between them.

Therefore, the general observations regarding the experimental values of the principal components of orientation tensor are as follows:

1. At the entrance region, region 1, the values of the a_{11} and a_{22} components of the orientation tensor are close ($\sim$0.5) due to the initial radial divergent flow pattern followed by the fibers. The near-zero value of the a_{33} component indicates that at this region there are some fibers still aligned in the thickness direction (see Figure 12).
2. At the lubrication region, region 2, a layered structure is observed. The high values of the a_{11} component ($\sim$0.8) are found near the walls of the box and the low values of a_{11} ($\sim$0.3) are found near its midplane, i.e. $z/H = 0.5$. The trend in the values of the a_{22} component is inverse to that of the a_{11} component. The value of the a_{33} component is practically null, indicating a planar fiber orientation (see Figure 13).

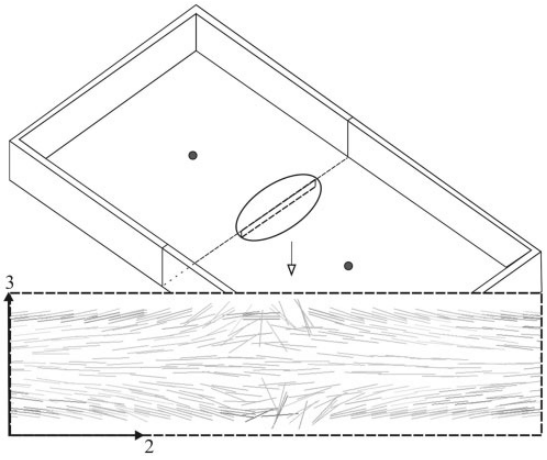

Figure 11. Predicted through-thickness fiber orientation along the cross flow direction at the WL region.

3. At the WL region, region 3, the a_{22} component of the orientation tensor displays its highest value (range from -0.6 to -0.9) due to the transverse alignment of the fibers. The variation profile of the a_{11} component through the thickness direction is flatter than in region 2, and in addition the value of this component is the minimum of the three regions. As in the entrance region, the a_{33} component has a near-zero value ($\sim$0.1). The alignment of the fibers in the thickness direction at this zone is associated to a "pole vaulting" phenomenon—which takes place when the flow fronts enter in contact—that orientates them out of the main flow plane[12–17] (see Figure 14).

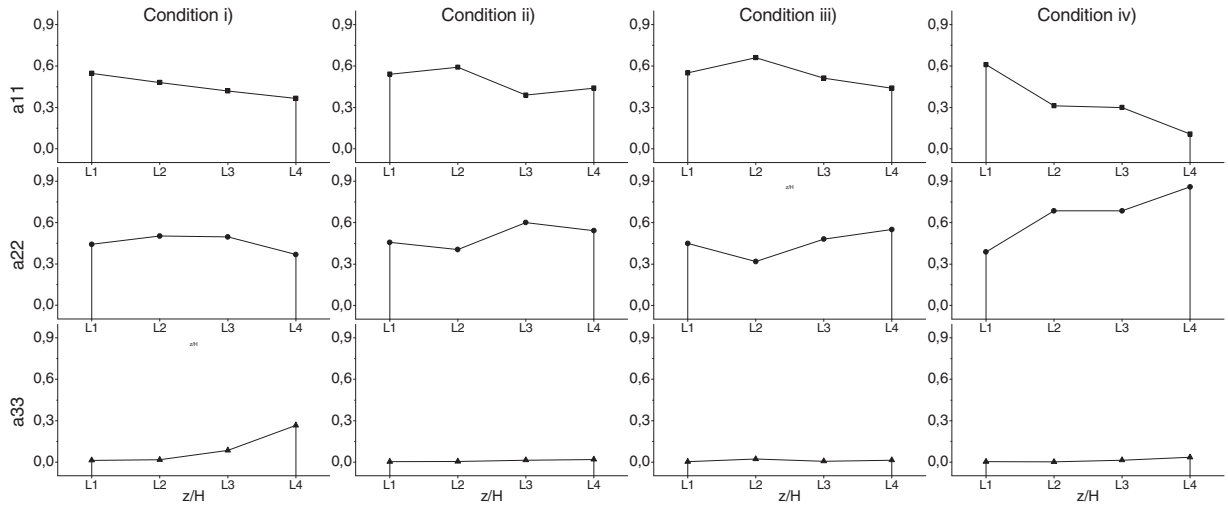

Figure 12. Experimental through-thickness FOD at the entrance region. (a) Condition (i), (b) condition (ii), (c) condition (iii), and (d) condition (iv).

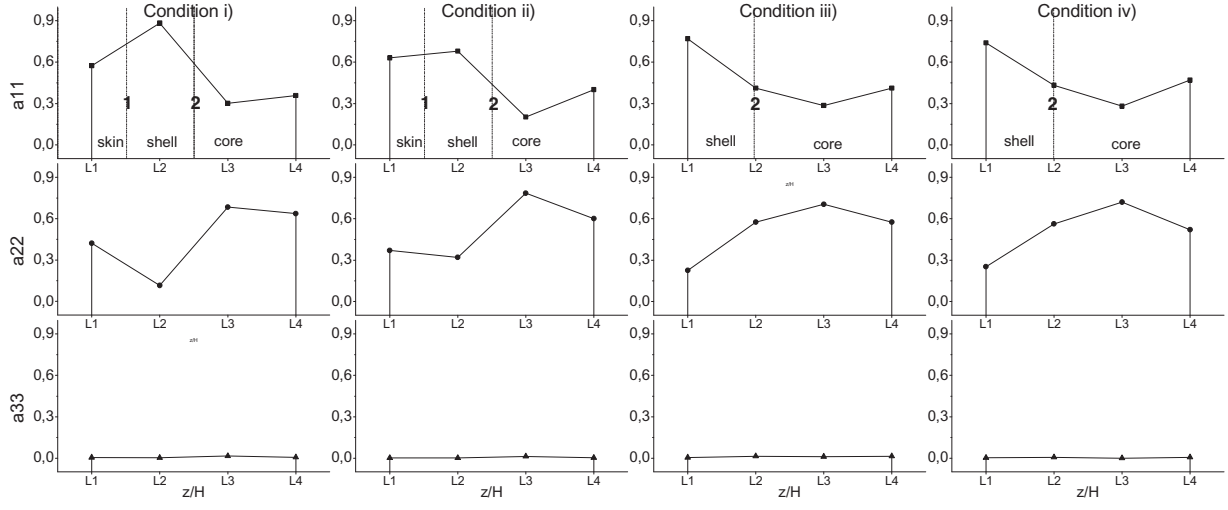

Figure 13. Experimental through-thickness FOD at the lubrication region. (a) Condition (i), (b) condition (ii), (c) condition (iii), and (d) condition (iv).

The through-thickness layered nature of the fiber orientation is only explained for the lubrication region—the fully developed flow zone—since it emerged from the previous analysis that the through-thickness profiles of the a_{11} component for the entrance and WL regions are substantially flat, meaning that the laminate fiber structure is not as much distinguishable as in region 2. Thus, the explanation is referred to in Figure 13 which displays the plots of the principal components of the orientation tensor as a function of the through-thickness position corresponding to this region. For the definition of the general shape of the a_{11} component, two vertical dashed lines labeled 1 and 2 are drawn in Figure 13, and the interceptions of these lines with the a_{11} values are used to define the layered structure. For clarity purpose, the through-thickness positions z/H for which the a_{11} values are maximum and minimum, respectively, are referred to as maximum and minimum z/H. Line 1 is set between $z/H = 0-L1$ and maximum z/H (only for conditions in which maximum a_{11} value is not at $z/H = 0$), see the a_{11} profile for conditions (i) and (ii). Line 2 is defined between maximum and minimum z/H, so this line is drawn for all the conditions. Between $z/H = 0$ and the line 1 the skin region is located. The shell region is between the line 1 and the line 2 and core region started at the line 2.

The experimental orientation distributions for conditions (i) Tm: 250°C, ti: 0.5 s and (ii) Tm: 250°C, ti: 1.5 s exhibit the classic five-layered laminate structure

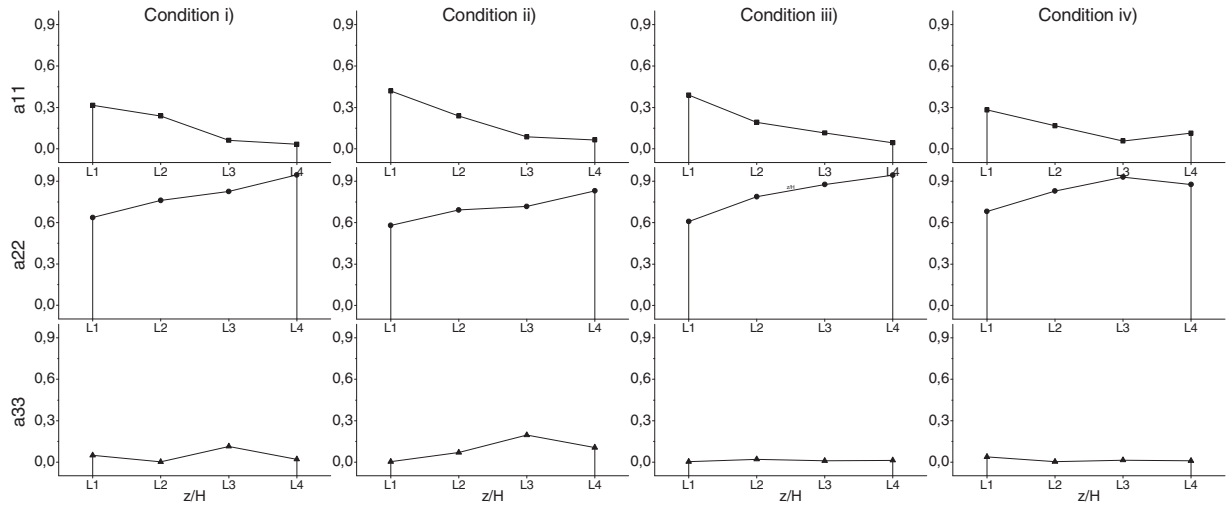

Figure 14. Experimental through-thickness FOD at the WL region. (a) Condition (i), (b) condition (ii), (c) condition (iii), and (d) condition (iv).

with two skin layers, two shell layers, and one core region between the shell layers (see Figure 13, conditions (i) and (ii)). Whereas the orientation distribution for conditions (iii) Tm: 280°C, ti: 0.5 s and (iv) Tm: 280°C, ti: 1.5 s is a three-layer laminate structure with two shell layers and one core between the shell layers (see Figure 13, conditions (iii) and (iv). The presence of the skin layer is directly associated to the process conditions. Particularly, it depends on cooling rate and filling time.[6,10] Several works indicate that lower melt temperatures lead to formation of thicker frozen layers.[6,10,24–26] Accordingly, in our case, frozen layers only appear in those samples injected at the low melt temperature (250°C). At the high melt temperature (280°C), heat transfer time is enough for the fibers to be aligned with the flow before they are frozen in the polymer. On the other hand, it is expected that an increase in the injection time will produce the same effect as a decrease in temperature,[10,24–26] i.e. a thicker frozen layer; however, the opposite effect was found in the experimental measurements of fiber orientation: sample injected under condition (i) presents a thicker frozen layer than sample injected under condition (ii) (slower injection speed) (see Figure 13, conditions (i) and (ii)).

Influence of process conditions on FOD

To study the variation on the degree of fiber orientation induced by changes in the processing parameters, a quantitative analysis of the sensitivity of the experimental a_{11} values as a function of the different combinations of the melt temperatures 250 and 280°C and injection times 0.5 and 1.5 s is done. For this purpose, Figure 14 displays the maximum, minimum, and through-thickness average values of the a_{11} component obtained for each process condition at regions 1–3.

As a general remark, no appreciable changes are found in the average value of a_{11} calculated for the different conditions at any of the three regions of interest, Figure 15. It is found that minimum a_{11} values at region 1 are lower for conditions (iii) and (iv) than for conditions (i) and (ii). This could be explained based on previous discoveries[24–26] which postulate that a higher melt temperature increases the grade of transversal orientation, and thus, produces a decrease in the a_{11} value. On the other hand, the maximum a_{11} value at the region 2 is higher for condition (i) than for the remaining conditions. Accordingly with the results found by other authors,[10,24–26] higher melt temperatures and lower injection times lead to an increase in fiber orientation.

The maximum and minimum values of the a_{11} component at the WL region show no significant variation due to changes in the processing condition. This is particularly important due to the fact that one of the many recommended ways to improve WL entanglement is to increase the melt temperature,[17] but in our case, this change did not produce an appreciable decrease in fiber orientation such as that produced in the entrance region before the same variation.

Quantitative comparison of experimental and predicted fiber orientations along the main, cross, and through-thickness flow directions

In Figure 16 experimental and predicted through-thickness averaged a_{11} component obtained for the regions 1–3—referred in the images as R1, R2, and R3—for each process condition is plotted. As it

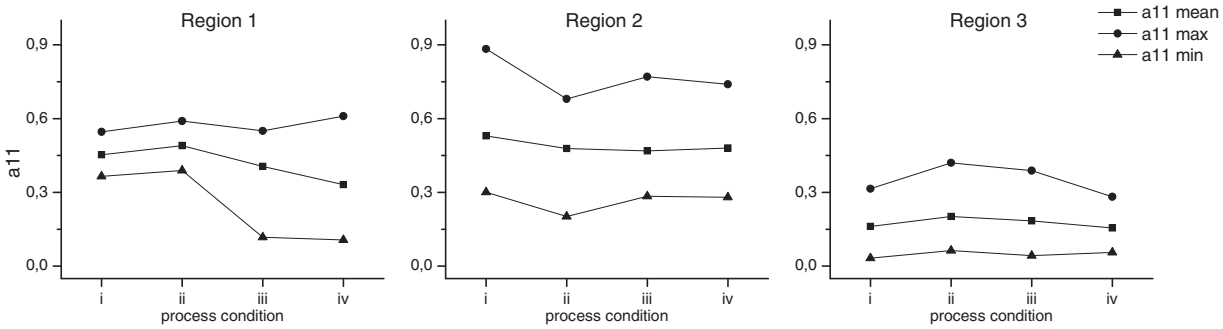

Figure 15. Experimental fiber orientation for the different process conditions for the entrance, lubrication, and WL regions. (a) Region 1, (b) region 2, and (c) region 3.

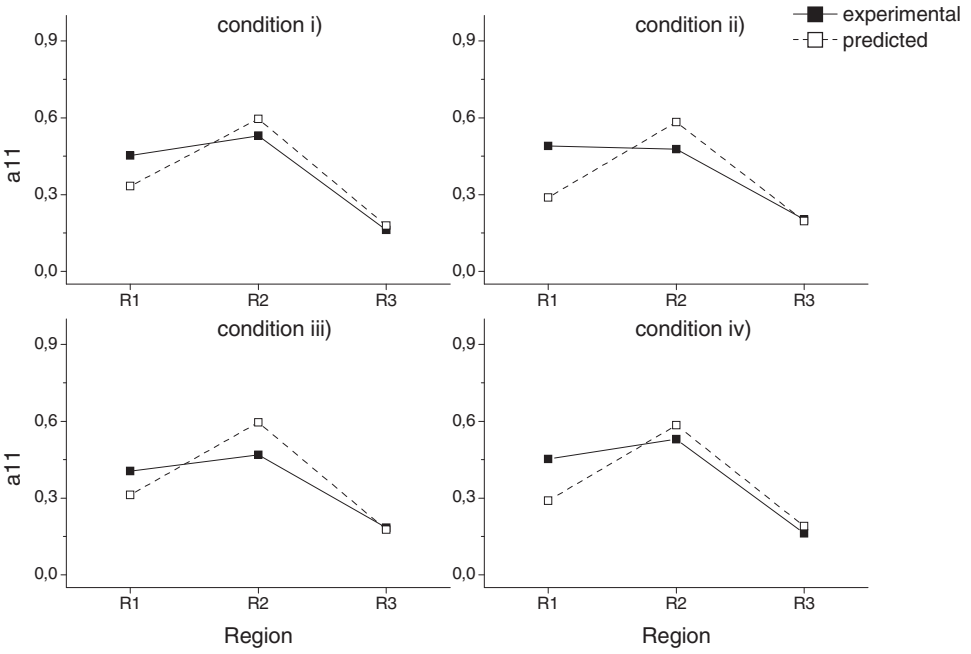

Figure 16. Comparison between experimental and predicted through-thickness average fiber orientation along the main flow direction. (a) Condition (i), (b) condition (ii), (c) condition (iii), and (d) condition (iv).

was qualitatively explained, the lubrication region (region 2) is characterized by a highly aligned fiber orientation, thus at this region the a_{11} value is the maximum of the three regions. At the WL region, the alignment of the fibers is mainly transversal to the main flow direction, being the a_{11} value at this region the minimum of the three regions. Predicted results show the same location of the maximum and minimum a_{11} values than in the experimental ones, but orientation degree is underestimated for region 1, and overestimated for region 2. The predicted and experimental through-thickness average a_{11} values at region 3 rightly match for all the conditions.

Figure 17 shows the plots of the experimental and predicted through-thickness averaged a_{11} component obtained for the central and border regions—referred in the images as central and border—at the region 2 and for each process condition. The fiber orientation decreases with the radial distance to the IP, thus, the a_{11} values are lower for the border region than for the central one. The experimental and predicted results show the same decrease in the a_{11} values, but for predicted results this change is slightly more abrupt—see the slopes of the curves.

Figure 18 shows the plots of the a_{11} component as a function of the through-thickness position at the lubrication region and for each process condition. The comparison of the experimental and predicted through-thickness fiber orientations is explained only for the region 2, for the same reason explained in the "Experimental through-thickness FOD" section.

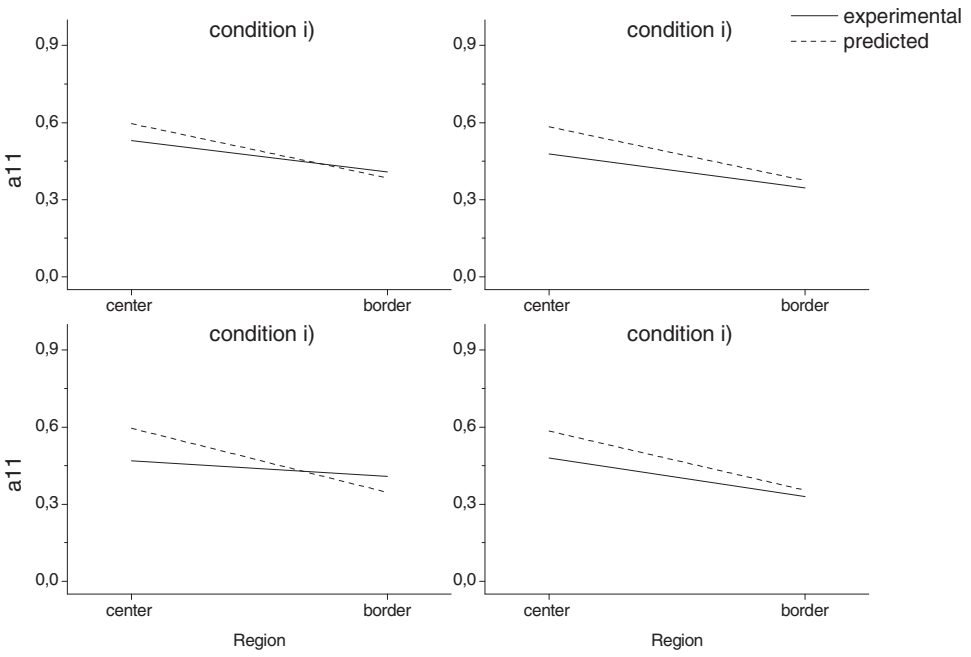

Figure 17. Comparison between experimental and predicted through-thickness average fiber orientation along the cross flow direction at the lubrication region. (a) Condition (i), (b) condition (ii), (c) condition (iii), and (d) condition (iv).

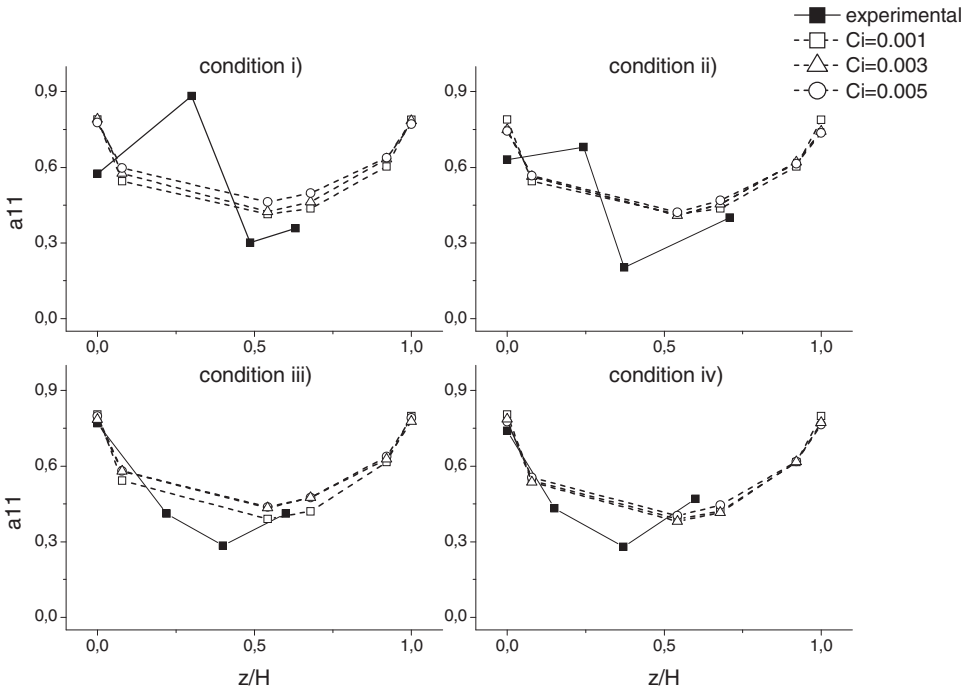

Figure 18. Comparison between experimental and predicted through-thickness FOD at the lubrication region. (a) Condition (i), (b) condition (ii), (c) condition (iii), and (d) condition (iv).

From the experimental results arises that the conditions (i) Tm: 250°C, ti: 0.5 s and (ii) Tm: 250°C, ti: 1.5 s display a five-layered laminate structure of fiber orientations (skin–shell–core) and the conditions (iii) Tm: 280°C, ti: 0.5 s and (iv) Tm: 280°C, ti: 1.5 s only present a three-layered structure (shell–core). On the other hand, it can be seen in Figure 18 that simulation fails in predicting the skin region for the low temperature conditions (i) and (ii) and the predicted alignment structure is three layered for all the conditions. This

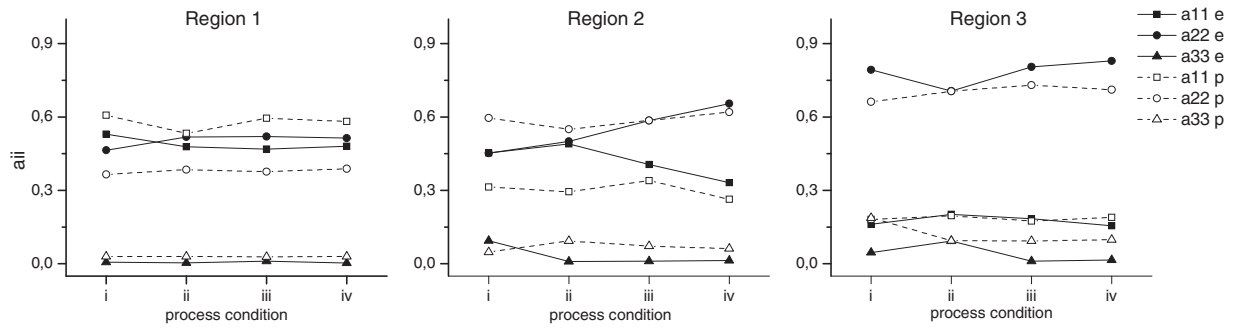

Figure 19. Principal components of the fiber orientation tensor for the different process conditions, for the entrance, lubrication, and WL regions. (a) Region 1, (b) region 2, and (c) region 3.

is deduced from the fact that at $z/H = 0$, i.e. at the wall of the box, the predicted a_{11} value is maximum constituting then the shell layer, not the skin which is characterized by a lower a_{11} value from that of the shell. As it has been demonstrated, the presence of a closure approximation for the fourth-order orientation tensor itself may introduce some error into the simulation results.[30,31] Then, it is the subject and motivation for a further work to determine if a change in the chosen approach model will effectively predict the skin layer.

From the analysis of the predicted and experimental values of the a_{11} components it is found that:

1. For the boxes injected at a high melt temperature 280°C, the predicted maximum a_{11} values in the shell layer match closely with those of the experimental data (−0.8) (see Figure 18, conditions (iii) and (iv)).
2. For the boxes injected at a low melt temperature 250°C, the predicted and experimental maximum a_{11} values are close, but they are located at different through-thickness positions: predicted maximum a_{11} values are at $z/H = 0$ whereas experimental values are shifted to a z position between the bottom and midplanes of the box (see Figure 18, conditions (i) and (ii)). This discrepancy is due to the presence of a skin layer not predicted by simulation.
3. For all of the conditions the minimum a_{11} values, i.e. those in the core, tend to be overpredicted by simulation. In our case, the experimental results show that fibers at the core are highly oriented transversely to the flow, leading to a lower value of the a_{11} component. The experimental minimum a_{11} values range from 0.2 to 0.4, whereas the predicted minimum a_{11} values are about 0.5. Predicted minimum a_{11} values are found at the midplane of the box, giving a symmetric through-thickness fiber distribution, while experimental minimum a_{11} values are shifted to a z position closer to the bottom plane of the box.

As it is expected a higher interaction coefficient would produce a randomized effect on the fibers, lowering its orientations; simulation trials with different higher interaction coefficients (0.003 and 0.005) were done in order to achieve a better fit of the predicted a_{11} minimum values to the experimental data. The results are also presented in Figure 18. It is found that a higher interaction coefficient produces a slight increase in the minimum a_{11} value and lowers the maximum a_{11} in a value by an amount that can be considered negligible. Thus, it can be remarked that in our work, the adjustment of the experimental minimum values cannot be achieved by the sole variation of the interaction coefficient.

Figure 19 is presented in order to resume the general trend in the variation of the experimental and predicted principal components of the orientation tensor for the three regions of interest and for the different process conditions. This figure displays the through-thickness averaged value of the a_{11}, a_{22}, and a_{33} components of the orientation obtained for each processing condition. As general remarks it can be pointed out that:

1. There is a consistent error in the simulation prediction of the average values of the a_{11} and a_{22} components of the orientation tensor at the entrance and lubrication regions, which can be attributed to the overestimation of the orientation at the core layer.
2. At the WL region, where the alignment of the fibers is predominantly unidirectional—along the cross flow direction—and the skin core structure is practically not distinguishable, it is found that the average values of the a_{11} and a_{22} components are very close.
3. The out-of-plane orientation is overestimated by the simulation prediction for all the regions and process conditions.

Conclusions

This work aims to experimentally validate the numerical simulation of FOD and the through-thickness layered structure performed by commercial CFD software

Moldex3D in a double-gated injection-molded glass fiber-filled (40 wt%) polypropylene box, processed at different combinations of melt temperature and injection time. The second-order orientation tensors have been deduced from experimental measurements of fiber orientation applying the method of ellipses and compared with the predicted ones by the commercial code. The modeling approach evaluated in this work consists in the implementation of the FT model with modified IBOF closure approximation for the fourth-order orientation tensor. The value of the interaction coefficient of the rotary diffusion model adopted is 0.001.

Regarding the experimental results, the box can be divided along the main flow direction into three regions of a distinctively fiber orientation, namely the entrance, lubrication, and WL regions. At the WL zone, the orientation is predominantly transversal to the main flow direction. The fiber orientation also changes with the radial distance from the IP, becoming less oriented from the central region of the box toward its edges or border region. At the lubrication region, there is a through-thickness distribution of fiber orientations. The boxes injected at the lower melt temperature display a five-layered laminate structure, skin–shell–core; while the boxes injected at the higher melt temperature present a three-layered laminate structure, shell–core. Process parameters do not strongly affect the grade of the orientation in any of the regions of interest but determine the distinctive layer structure of fiber orientation at the lubrication region.

The simulation accurately predicts the radial divergent flow pattern of the fibers and its qualitative orientation along the main, cross, and through-thickness flow directions but fails in predicting the skin region developed at the lowest temperature condition tried. This could be attributable to inherent errors of the modeling approach introduced by the use of a closure approximation for the fourth-order orientation tensor. The ongoing work is devoted to evaluate the accuracy of different closure approximations and rotary diffusion models.

Predicted maximum values of the a_{11} components match closely with the experimental ones, but the minimum a_{11} values tend to be much overestimated for all the conditions. The fit of the minimum values cannot be improved by changing the interaction coefficient as expected.

The out-of-plane orientation is overpredicted for all the regions and for all process conditions.

The orientation distribution pattern is heterogeneous since it varies according to the location in the specimen. It has been shown that the interaction coefficient of the rotary diffusion model depends not only on the content and shape of the fibers, but also and fundamentally on the orientation state. Due to the fact that the fiber orientation changes along the main, cross, and through-thickness flow directions, the modeling approach for the fiber orientation cannot fit all of the orientation tensor components at every region.

It is usually accepted that in order to obtain easy assessable fiber orientation parameters that could be useful to industrial evaluation, it is essential to comprehend and to be able to predict the nature of the flow field inside a mold and the flow-induced variation of the fiber orientation for effective design of short fiber-reinforced plastic parts. Nevertheless, our findings make evident the importance of knowing the experimental distribution of fibers in model pieces that presents complex geometric features, which allows establishing the limitations of predictive models that can be useful to reliably design real industrial pieces, in which this type of detailed characterization is almost not possible.

Declaration of conflicting interests

The author(s) declared no potential conflicts of interest with respect to the research, authorship, and/or publication of this article.

Funding

The author(s) disclosed receipt of the following financial support for the research, authorship, and/or publication of this article: The authors would like to acknowledge financial support from the National Agency for Science and Technology Promotion of Argentina (grant number PICT-2013-1711)

References

1. Jeffery GB. The motion of ellipsoidal particles immersed in a viscous fluid. *Proc Roy Soc* 1922; 102: 161–179.
2. Folgar F and Tucker CL III. Orientation behavior of fibers in concentrated suspensions. *J Reinf Plast Compos* 1984; 3: 98–119.
3. Chung ST and Kwon TH. Coupled analysis of injection molding filling and fiber orientation, including in-plane velocity gradient effect. *Polym Compos* 1996; 17: 859–872.
4. Advani AG and Tucker CL III. The use of tensors to describe and predict fiber orientation in short fiber composites. *J Rheol* 1987; 31: 751–784.
5. Bay RS and Tucker CL III. Fiber orientation in simple injection moldings. Part I: theory and numerical methods. *Polym Compos* 1992; 13: 317–331.
6. Gupta M and Wang KK. Fiber orientation and mechanical properties of short-fiber-reinforced injection-molded composites: simulated and experimental results. *Polym Compos* 1993; 14: 367–382.
7. Tucker CL III and Advani SG. *Flow and rheology in polymer composites manufacturing*. Vol. 10. 1st ed. Amsterdam: Elsevier, 1994.

8. Ko J and Youn JR. Prediction of fiber orientation in the thickness plane during flow molding of short fiber composites. *Polym Compos* 1995; 16: 114–124.
9. Greene JP. Numerical analysis of injection molding of glass fiber reinforced thermoplastics. Part 2: fiber orientation. *Polym Eng Sci* 1997; 37: 1019–1035.
10. Papthanasiou TD. Flow-induced alignment in injection molding of fiber reinforced polymer composites. In: Papthanasiou TD and Guell DC (eds) *Flow-induced alignment in composite materials*, 1997.
11. Larsen A. Injection molding of short fiber reinforced thermoplastics in a center-gated mold. *Polym Compos* 2000; 21: 51–64.
12. Vaxman A, Narkis M and Siegman A, et al. Weld line characteristics in short fiber reinforced thermoplastics. *Polym Compos* 1991; 12: 161–168.
13. Kyoo L and Tetsuo S. Fiber orientation of polymer injection weld and its strength evaluation. *KSME J* 1993; 7: 173–181.
14. Nabi ZU and Hashemi S. Influence of short glass fibres and weldlines on the mechanical properties of injection-moulded acrylonitrile–styrene–acrylate copolymer. *J Mater Sci* 1998; 33: 2985–3000.
15. Chrysostomou A and Hashemi S. Mechanical properties of injection moulded styrene maleic anhydride (SMA) Part II Influence of short glass fibres and weldlines. *J Mater Sci* 1998; 33: 4491–4501.
16. Gamba MM, Pouzada S and Frontini PM. Impact properties and microhardness of double-gated glass-reinforced polypropylene injection moldings. *Polym Eng Sci* 2009; 49: 1688–1695.
17. Kuehnert I, Spoerer Y and Zimmermann M. Weld lines in injection molded parts: strength, morphology and improvement. In: *SPE ANTEC*, Indianapolis, EEUU, 23–25 May 2016, pp.1255–1258.
18. Patcharaphun S. *Characterization and simulation of material distribution and fiber orientation in sandwich injection molded parts*. PhD Thesis. Chemnitz University of Technology, Bangkok, 2006.
19. Velez García G. *Experimental evaluation and simulations of fiber orientation in injection molding of polymers containing short glass fibers*. PhD Thesis, Virginia Polytechnic Institute and State University, Virginia, 2012.
20. Han K-H and Taek C-Y. Numerical simulation of three-dimensional fiber orientation in injection molding including fountain flow effect. *Polym Compos* 2002; 23: 222–238.
21. Wang J and Jin X. Comparison of recent fiber orientation models in autodesk moldflow insight simulation with measured fiber orientation data. In: *Proceedings of the polymer processing society 26th annual meeting*, Banff, 2010.
22. Hsu C-C, Hsieh D-D, Chiu H-S, et al., Investigation of fiber orientation in filling and packing phases. In: *Molding innovation*, Lowell, 2012.
23. Foss PH, Tseng HC, Snawerdt J, et al. Prediction of fiber orientation distribution in injection molded parts using moldex3D simulation. *Polym Compos* 2013; 35: 671–680.
24. Xavier SF, Tyagi D and Misra A. Influence of injection-molding parameters on the morphology and mechanical properties of glass fiber-reinforced polypropylene composites. *Polym Compos* 1982; 3: 88–96.
25. Singh P and Kamal MR. The effect of processing variables on microstructure of injection molded short fiber reinforced polypropylene composites. *Polym Compos* 1988; 10: 344–351.
26. Shokri P and Bhatnagar N. Effect of melt and mold temperature on fiber orientation during flow in injection molding of reinforced plastics. *IPP* 2006; 21: 480–486.
27. Clarke A, Davidson N and Archenhold G. Measurements of fibre direction in reinforced polymer composites. *J Microsc* 1993; 171: 69–79.
28. Pontes AJ, Neves NM and Pouzada AS. The role of the interaction coefficient in the prediction of the fiber orientation in planar injection moldings. *Polym Compos* 2003; 24: 358–366.
29. Larson RG. *The structure and rheology of complex fluids*. New York: Oxford University Press, 1999. [WorldCat]
30. Dray D, Gilormini P and Regnier G. Comparison of several closure approximations for evaluating the thermoelastic properties of an injection molded short-fiber composite. *Compos Sci Technol* 2007; 67: 1601–1610.
31. Chung DH and Kwon TH. Applications of recently proposed closure approximations to injection molding filling simulation of short-fiber reinforced plastics. *Korea-Aust Rheol J* 2000; 12: 125–133.